Evaluation of near-threshold fatigue crack propagation in harmonic-structured CP titanium with a bimodal grain size distribution

Kikuchi, Shoichi ; Mori, Tetsuya ; Kubozono, Hiroki ; Nakai, Yoshikazu ; Kawabata, Mie Ota ; Ameyama, Kei

(Citation)
Engineering Fracture Mechanics,181:77-86

(Issue Date)
2017-08

(Resource Type)
journal article

(Version)
Accepted Manuscript

(URL)
https://hdl.handle.net/20.500.14094/90004627

Title page

Evaluation of Near-threshold Fatigue Crack Propagation in Harmonic-structured CP Titanium with a Bimodal Grain Size Distribution

Shoichi KIKUCHI [a,*], Tetsuya MORI [a], Hiroki KUBOZONO [a], Yoshikazu NAKAI [a],

Mie Ota KAWABATA [b], and Kei AMEYAMA [b]

[a] Department of Mechanical Engineering, Graduate School of Engineering, Kobe University, 1-1 Rokkodai-cho, Nada-ku, Kobe, 657-8501, JAPAN

[b] Department of Mechanical Engineering, College of Science and Engineering, Ritsumeikan University, 1-1-1 Noji-higashi, Kusatsu, Shiga, 525-8577, JAPAN

*: Corresponding author

E-mail address: kikuchi@mech.kobe-u.ac.jp,

Phone: +81-78-803-6329, Fax: +81-78-803-6155

Abstract

To examine near-threshold fatigue crack propagation in commercially pure (CP) titanium with a bimodal harmonic structure, which is defined as a coarse grained structure surrounded by a network of fine grains, *K*-decreasing tests were conducted. The crack growth rates for harmonic-structured CP titanium were higher than those for homogeneous material with coarse grains at comparable stress intensity range, while the threshold stress intensity range was lower. This phenomenon was attributed to a reduction in the extent of crack closure and the effective threshold stress intensity range, resulting from the presence of fine grains in the harmonic structure.

Keywords

Fatigue, Fracture mechanics, Commercially pure titanium, Crack closure, Grain refinement

1. Introduction

Various metallic materials, including stainless steels, cobalt alloys, magnesium alloys, titanium alloys and commercially pure (CP) titanium, have been previously investigated as biomaterials [1-7] for the replacement of bone tissue. CP titanium is of particular interest in this regard since it exhibits good biocompatibility and high corrosion resistance, and does not contain toxic elements such as Cr, Al or V. However, this material has lower tensile strength and fatigue strength than titanium alloys [1-4], and so improving the mechanical properties of CP titanium has become an important topic. The mechanical properties of metallic materials are affected by their microstructure, and grain refinement has been shown to be an effective method for increasing the strength of CP titanium [4,8-15].

The homogeneous fine-grained structure resulting from severe plastic deformation typically decreases the ductility of a metal [11,14-18], including that of CP titanium [11,14,15], via the early induction of plastic instability. Previous investigations have demonstrated that a new microstructural design can improve both the strength and ductility (or toughness) of some metallic materials [8,14-31]. As an example, Sergueeva et al. [8] reported that both the strength and elongation of CP titanium were improved by high-pressure torsion followed by brief low temperature annealing. Our own research group [24-31] has developed a harmonic structure concept for the fabrication of titanium-based materials with high strength and ductility, based on powder metallurgy. This process generates a coarse grained structure surrounded by a network of fine grains. CP titanium [24-27] with a

harmonic structure has exhibited higher strength and ductility than homogeneous specimen with coarse microstructures. This microstructure design technique can control the grain size distribution by varying several process parameters [25,27,28,30].

Another important aspect of the mechanical properties of biomaterials is fatigue resistance, which is dependent on the microstructure and stress ratio (the ratio of the minimum to the maximum stress) [4,10-13,28-39]. Kitahara et al. [11] determined that the characteristics of fatigue crack propagation in CP titanium are affected by the microstructure, and that the threshold stress intensity range, ΔK_{th}, decreases as the grain size decreases with increasing number of accumulative roll bonding cycles. Our prior work focused on the fatigue properties of a Ti-6Al-4V alloy with a bimodal harmonic structure and demonstrated that the fatigue limit in this alloy was higher than that for homogeneous analogues [28,29], while the fatigue threshold associated with long crack propagation was reduced [30,31]. Therefore, it would be helpful to examine the effects of a bimodal grain size distribution on fatigue crack propagation in harmonic-structured CP titanium, to assist in obtaining properties suitable for practical medical and biological engineering applications.

The purpose of the present study is to examine near-threshold fatigue crack propagation in harmonic-structured CP titanium with a bimodal grain size distribution, since this material is known to exhibit superior mechanical properties. The effect of grain size on fatigue crack propagation at different stress ratios and the associated mechanism were also investigated using the crack closure concept, fractography and crystallography.

2. Experimental procedure

2.1 Material

CP titanium containing 0.004% C, 0.04% Fe, 0.015% N, 0.111% O, 0.012% H (all by mass, with the remainder being titanium) was employed in the present study. This metal was made into a powder (150 μm particle diameter) using the plasma rotating electrode process [40]. Fig. 1 demonstrates a schematic illustration of the process by which a harmonic-structured material with a bimodal grain size distribution was fabricated via MM and spark plasma sintering (SPS). As the mechanically milled powder containing fine surface grains undergoes SPS, each fine grained region is consolidated, just as in conventional sintering. The resulting network structure, shown in Fig. 1(c), is referred to as a harmonic structure. Mechanical milling (MM) to form fine grains at the powder particle surfaces was performed using a planetary ball mill with SUJ2 steel balls in an Ar atmosphere for 360 ks. The powders were subsequently consolidated by SPS at 1073 K for 0.6 ks under vacuum less than 15 Pa, and 50 MPa applied pressure using a 25 mm internal diameter graphite die to produce the specimens referred to herein as the MM series. Sintered materials fabricated from the as-received initial powder (referred to herein as the Untreated series) were also prepared for comparison purposes. The MM series exhibited almost the same elongation as the Untreated series, but higher 0.2% proof stress and tensile strength values in results of a prior study [41].

In addition, samples of bulk titanium containing 0.01% C, 0.10% O, 0.004% N, and

0.02% Fe (all by mass, with Ti as the balance) were used in this study to examine the effect of grain size on fatigue crack propagation in CP titanium. Two types of bulk materials were prepared. One was a coarse grained titanium that was used as-received (the C-Bulk series) while the other was a fine grained titanium (the F-Bulk series) that was cold-rolled to a 50% reduction and subsequently annealed at 873 K for 18 ks. The microstructures of the sintered compacts and bulk materials were characterized using electron backscattered diffraction (EBSD).

A flowchart summarizing the specimen preparation procedure is presented in Fig. 2. A total of four specimen types with different microstructures were prepared.

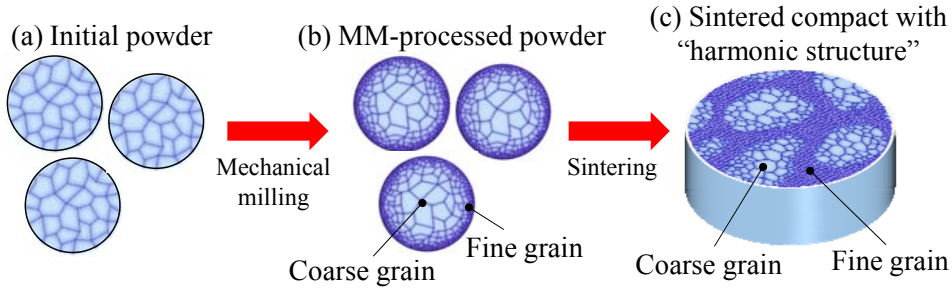

Fig.1 Schematic illustration of process for formation of harmonic-structured material.

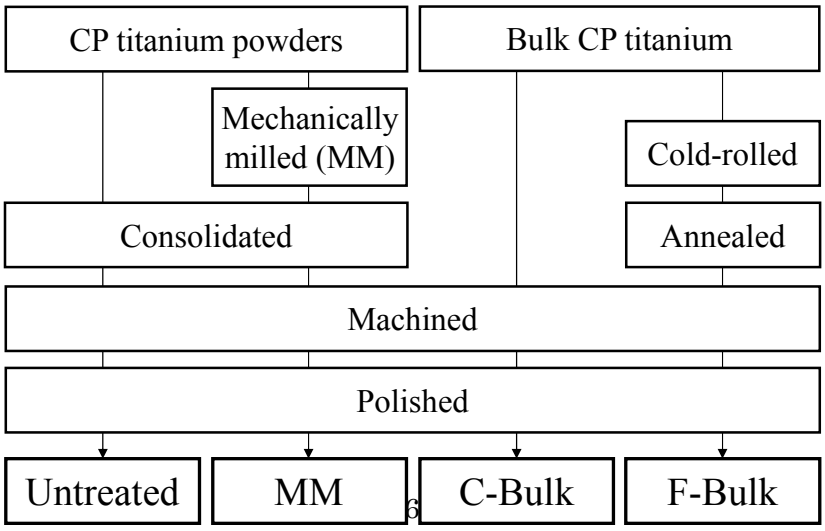

Fig.2 Flowchart of specimen preparation procedure.

2.2 Fatigue crack propagation test

The present study employed disk-shaped compact (DC(T)) specimens (2 mm thick) based on the ASTM standard. *K*-decreasing tests were conducted in ambient air with three different values of the stress ratio, *R*, of 0.1, 0.5 and 0.7 to approach the fatigue threshold of the specimens. Fatigue crack propagation tests were conducted at the same conditions as the previous study to compare the behavior of Ti-6Al-4V alloy. The magnitude of crack closure was monitored by the unloading elastic compliance method [42]; closure stress intensity K_{cl} was obtained from the closure load P_{cl}. The details can be found elsewhere [30]. Following the crack propagation tests, the fracture surfaces and crack profiles were observed by scanning electron microscopy (SEM) to elucidate the fatigue crack propagation mechanism.

3. Results

3.1 Microstructural characterization of CP titanium

Inverse pole figure (IPF) maps obtained by EBSD analysis for the (a) Untreated and (b) MM series are shown in Fig. 3. The Untreated series evidently contains coarse grains (Fig. 3(a)), whereas the MM series is composed of both fine and coarse equiaxed grains (Fig. 3(b)). The fine grains form a continuous three-dimensional network structure that surrounds the coarse grains. The most significant difference between this harmonic structure and a conventional bimodal structure is that all the fine-grained regions are interconnected in a continuous network.

Table 1 summarizes the average grain size and the area of the fine-grained microstructure for the MM series. The average grain size for the MM series (19.5 μm) was smaller than that for the Untreated series (122 μm), in which the majority of grains were coarse, as shown in Fig. 3(a). This difference occurred because grain refinement proceeded at the powder particle surfaces due to the increased strain induced by the MM process. This increased strain in turn decreased the average grain size in the fine grained structures, which are defined as grains less than 10 μm in size, of the sintered compacts (Table 1(b)). Furthermore, the average grain size in the coarse grained structure was also lower (Table 1(c)), implying that grains in the interiors of the powder particles were reduced in size during MM.

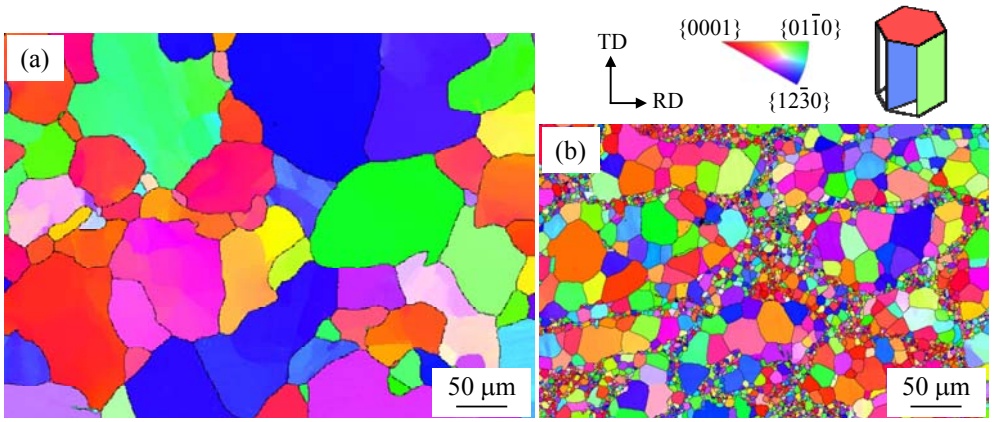

Fig.3 Inverse pole figure maps obtained by EBSD analysis for (a) Untreated and (b) MM series.

Table 1 Average grain size and areal fraction for fine-grained structure in MM series.

(a) Average grain size in entire microstructure, μm	19.5
(b) Average grain size in fine grained structure, μm	5.2
(c) Average grain size in coarse grained structure, μm	25.9

(d) Areal fraction of fine grained structure, %	31.0

Fig. 4 provides IPF maps obtained from EBSD analysis of the bulk materials. Maps are provided for the (a) as-received material (C-Bulk series), (b) 50% cold-rolled material, and (c) annealed material pre-treated with cold rolling (F-Bulk series). The average grain size for the C-Bulk series was 47 μm (Fig. 4(a)). In contrast, the IPF map for the cold-rolled material is of poor quality because of the high degree of strain induced by cold rolling (Fig. 4(b)), whereas Fig. 4(c) demonstrates that fine equiaxed grains with an average size of 10 μm were formed in the subsequently annealed material (F-Bulk series). It is therefore evident that bulk homogeneous materials with different grain sizes were prepared.

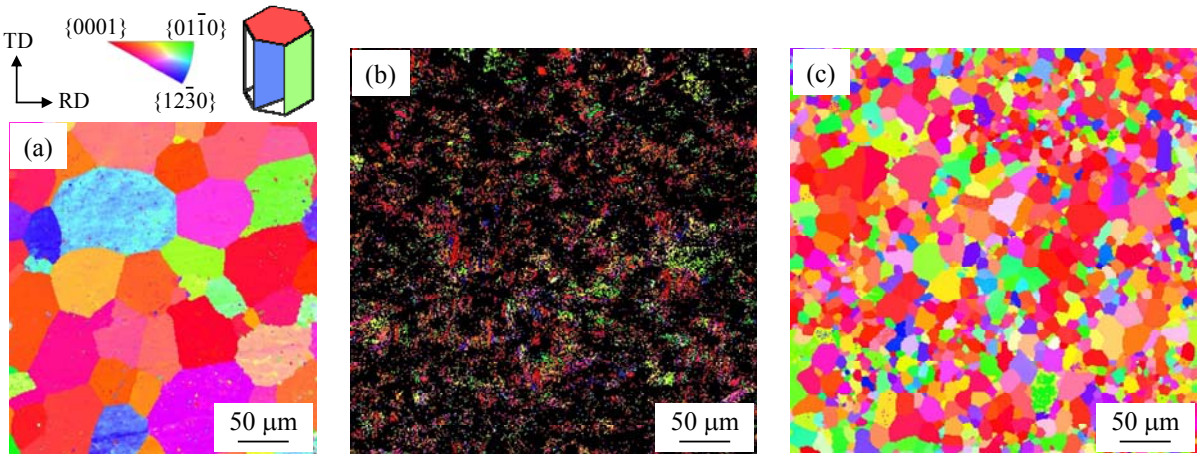

Fig.4 Inverse pole figure maps obtained by EBSD analysis for (a) as-received material (C-Bulk series), (b) cold-rolled material, and (c) annealed material pre-treated with cold rolling (F-Bulk series).

3.2 Effect of stress ratio on fatigue crack propagation in CP titanium sintered compacts

Fig. 5 plots the crack growth rate, da/dN, for the Untreated and MM series against ΔK, for stress ratios of R = 0.1, 0.5 and 0.7. In both series, ΔK_{th} exhibits a tendency to decrease with increasing R, while da/dN increases with increasing ΔK. Furthermore, the da/dN values for the MM series are consistently higher than those for the Untreated specimens at comparable ΔK levels. The relationship between ΔK_{th} and R for the sintered compacts is summarized in Fig. 6. The ΔK_{th} value decreases approximately linearly with increasing R. The relationship between ΔK_{th} and R for both series can be expressed by:

Untreated series: $\Delta K_{th} = -1.98R + 4.24$, and (2)

MM series: $\Delta K_{th} = -2.34R + 3.83$. (3)

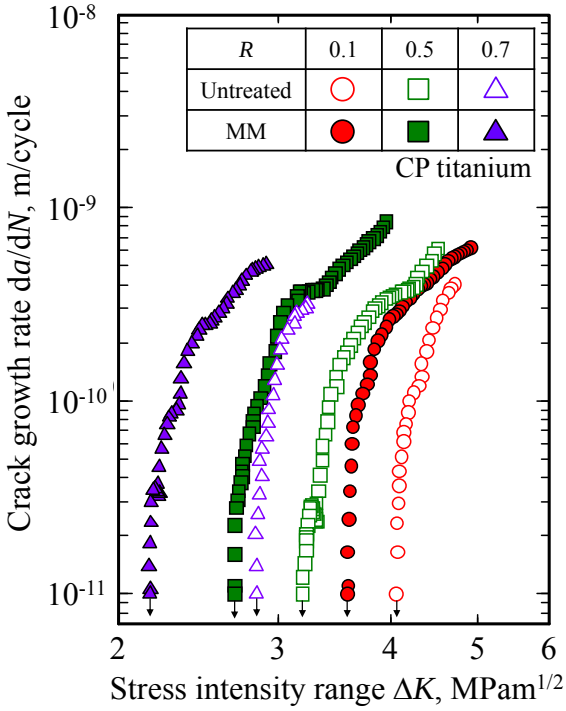

Fig.5 Relationship between crack growth rate and stress intensity range for various sintered compacts.

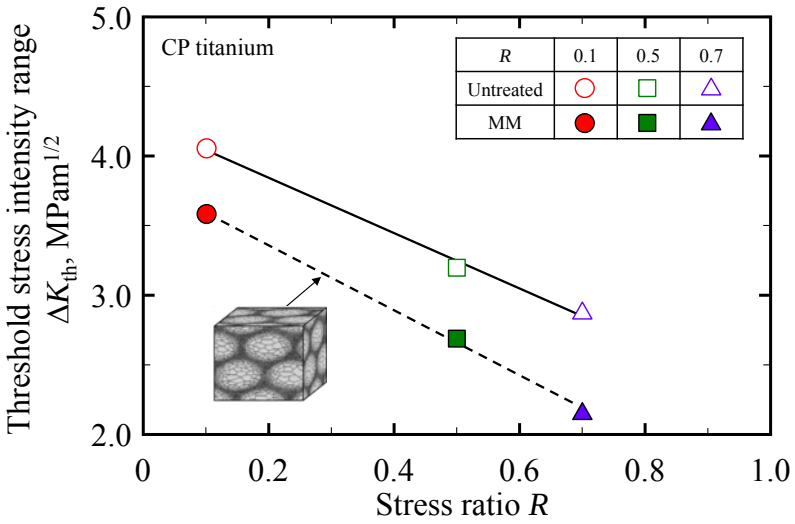

Fig.6 Relationship between threshold stress intensity range and stress ratio for various sintered compacts.

The ΔK_{th} values for the Untreated series were higher than those for the MM series at comparable stress ratios. However, the absolute value of the slope obtained by plotting the MM series data (2.34) was higher than that for the Untreated series (1.98), indicating that the stress ratio has a greater effect on near-threshold fatigue crack propagation in the MM series. It is also evident that the fatigue threshold for CP titanium was significantly reduced at a relatively high stress ratio due to the formation of a harmonic structure.

3.3 Crack closure in CP titanium sintered compacts

The effect of the stress ratio at near-threshold levels is generally attributed to crack closure [35]; therefore, ΔK_{eff} values were determined for the various CP titanium sintered

compacts. Fig. 7 plots da/dN against ΔK_{eff} for the Untreated and MM series. In the case of the Untreated series, the data series tend to converge to form a single plot near the threshold, although the da/dN values are slightly different. This result indicates that the stress ratio has a minimal effect on effective threshold stress intensity range, $\Delta K_{eff,th}$, in coarse grained CP titanium. In contrast, the $\Delta K_{eff,th}$ values for the MM series, each of which had a fine-grained structure, varied depending on the stress ratio and tended to decrease with increasing R.

To examine the effects of the stress ratio and microstructure on the crack closure magnitude, the ratio of the closure stress intensity factor, K_{cl}, to the maximum stress intensity factor, K_{max}, was calculated for each specimen. Fig. 8 presents the relationship between K_{cl}/K_{max} and ΔK_{eff} for the CP titanium sintered compacts at various stress ratios. In this figure, the K_{cl}/K_{max} value equals R in the case of samples for which there was no crack closure. The K_{cl}/K_{max} values for both series were evidently independent of ΔK_{eff} at a high stress ratio of 0.7, signifying that there was no crack closure. In contrast, at R values lower than 0.5, K_{cl}/K_{max} tended to increase with decreasing ΔK_{eff}. Moreover, the K_{cl}/K_{max} values for the MM series were lower than those for the Untreated series at low stress ratios (0.1 and 0.5). These results demonstrate that the presence of a harmonic structure reduced the extent of crack closure in the CP titanium sintered compacts, thus lowering ΔK_{th}. This same effect, in which a bimodal harmonic structure affects crack closure, has also been observed with Ti-6Al-4V alloy [31].

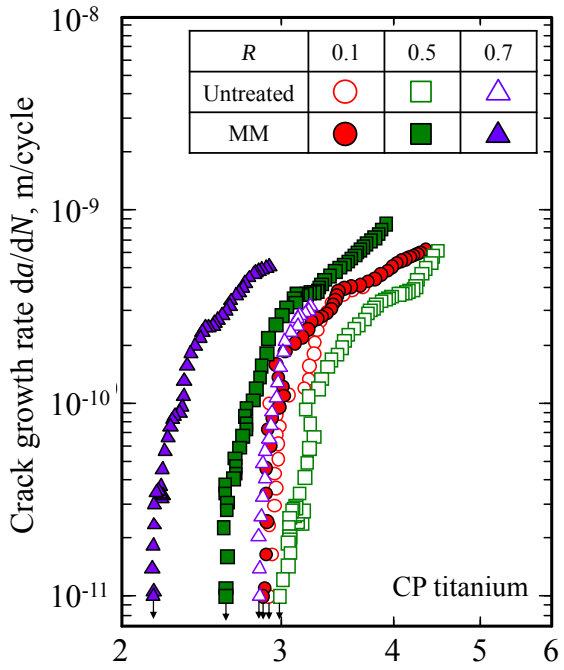

Fig.7 Relationship between crack growth rate and effective stress intensity range for various sintered compacts.

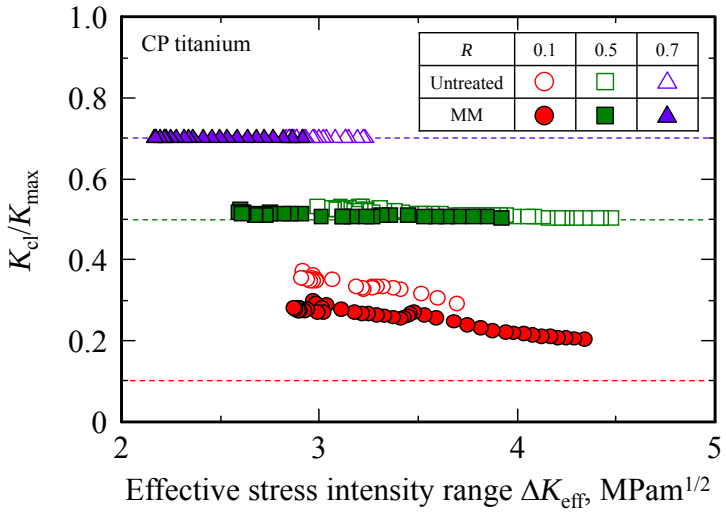

Fig.8 Relationship between K_{cl}/K_{max} and effective stress intensity range for various sintered compacts.

The crack profiles were observed using SEM because crack closure at near-threshold

levels is generally attributed to a roughness-induced mechanism [38,39]. Fig. 9 shows typical crack profiles for the (a) Untreated and (b) MM series, following tests at R = 0.5. These images confirm that the crack profile was affected by the microstructure. It can also be seen that the Untreated series displays a more tortuous and deflected crack path than the MM series. EBSD analysis of the MM series after testing found that the fatigue cracks did not preferentially propagate in the networked fine-grained structures, but rather traveled through the coarse-grained regions. Three-dimensional axonometric drawings were generated to characterize the surface topography of the fracture surfaces, and Fig. 10 presents typical drawings for the (a) Untreated and (b) MM series following tests at R = 0.1. Here it can be seen that the surface topography for the Untreated series was rougher than that for the MM series. Coarser microstructures are associated with more tortuous and more highly deflected crack paths [32], resulting in increased fatigue crack growth resistance due to roughness-induced crack closure.

Consequently, tortuous, deflected crack paths were suppressed in the bimodal harmonic structures, thus decreasing the crack closure magnitude, as shown in Fig. 8.

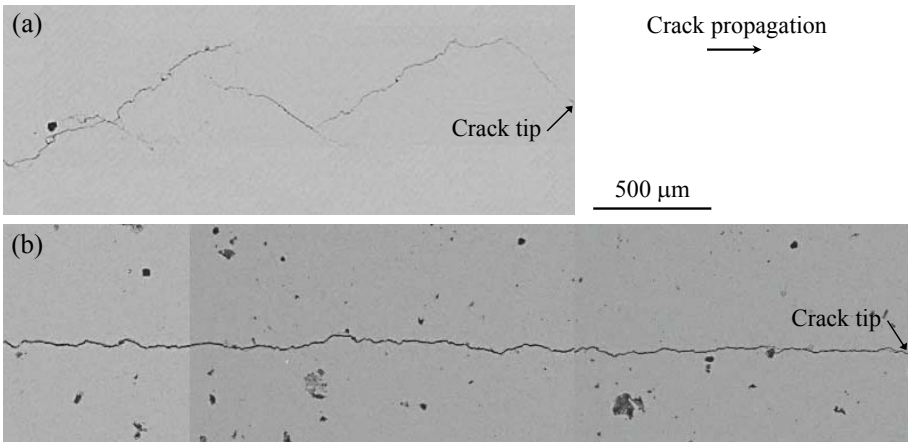

Fig.9 SEM micrographs of crack profiles for (a) Untreated and (b) MM series after testing at $R = 0.5$.

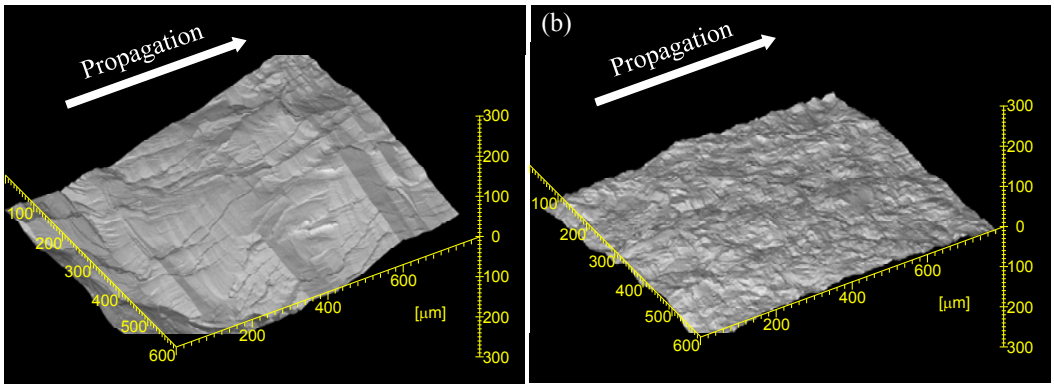

Fig.10 Axonometric drawings of fracture surfaces for (a) Untreated and (b) MM series after testing at $R = 0.1$.

4. Discussion

The ΔK_{th} values for the MM series with bimodal harmonic structures were consistently lower than those for the Untreated series (Figs. 5 and 6) at comparable stress ratios, due to a decrease in the crack closure magnitude (Fig. 8). Furthermore, the $\Delta K_{eff,th}$ values for the MM series were also lower than those for the Untreated series at comparable stress ratios (Fig. 7). It therefore appears that a harmonic structure reduces the fatigue threshold in CP titanium by eliminating the crack closure phenomenon. In this section, the effects of the grain size on fatigue crack propagation in bulk homogeneous CP titanium are assessed. Examining these effects allows us to find the reasons for the decreased fatigue threshold for the CP titanium sintered compacts containing both fine- and coarse-grained structures.

The relationship between ΔK_{th} and R for both bulk homogeneous materials are plotted in Fig. 11. For both series, ΔK_{th} decreases approximately linearly with increasing R as:

C-Bulk series: $\Delta K_{th} = -0.82R + 2.39$, and (4)

F-Bulk series: $\Delta K_{th} = -0.97R + 2.37$. (5)

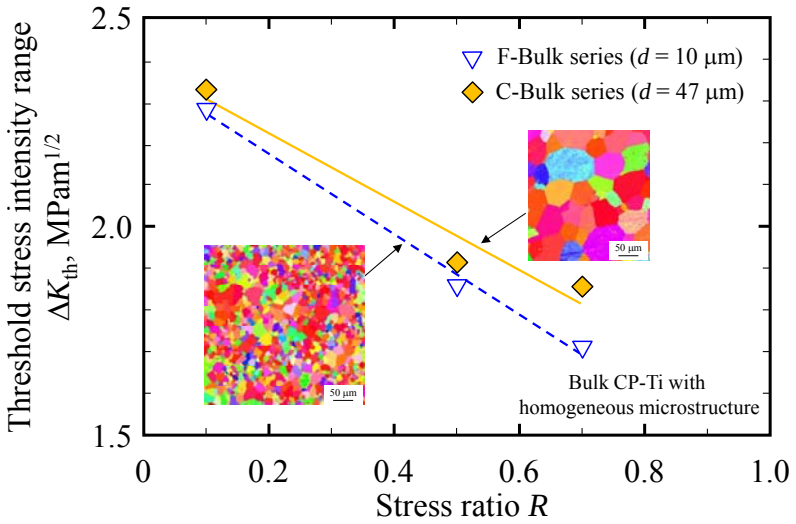

Fig.11 Relationship between threshold stress intensity range and stress ratio for two types of bulk homogeneous materials.

The ΔK_{th} values for the C-Bulk series were higher than those for the F-Bulk series at comparable stress ratios. However, the absolute value of the slope for the F-Bulk series data (0.97) was larger than that for the C-Bulk series (0.82), indicating that the stress ratio has a significant effect on near-threshold fatigue crack propagation in fine-grained CP titanium.

In the case of the bulk homogenous materials, crack closure occurred only at an R value of 0.1, and so K_{cl} was calculated for these samples at R = 0.1. Fig. 12 shows the relationship between K_{cl} and ΔK for the bulk homogeneous materials. The K_{cl} values for

C-Bulk series exhibit a tendency to decrease with decreasing ΔK. In contrast, K_{cl} for the F-Bulk series is roughly constant at 0.55 MPa $m^{1/2}$, a value that is lower than that for the C-Bulk specimens. These data demonstrate that the grain size strongly influences crack closure in CP titanium and that a fine-grained structure reduces the value of K_{cl}.

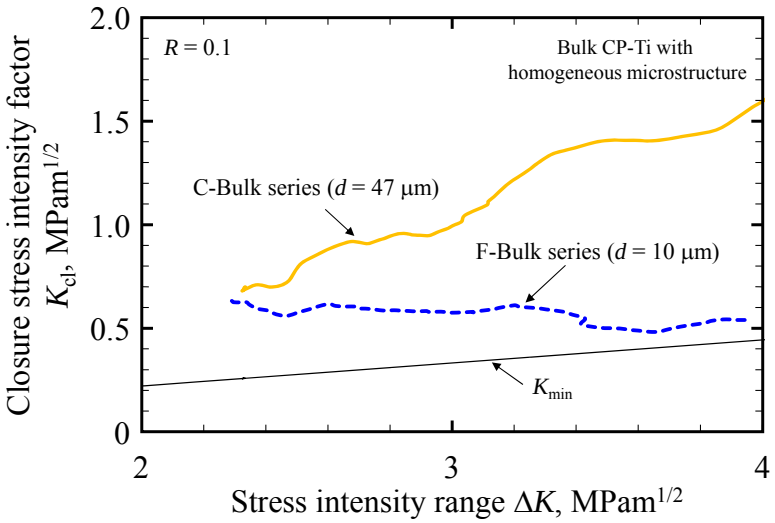

Fig.12 Relationship between closure stress intensity factor and stress intensity range for two types of bulk homogeneous materials.

Fig. 13 plots $\Delta K_{eff,th}$ at R = 0.1, 0.5 and 0.7 as a function of the square root of the grain size for bulk homogeneous CP titanium specimens with different grain sizes. $\Delta K_{eff,th}$ is equal to ΔK_{th} at R = 0.5 and 0.7 for both series because no crack closure occurred. In the case of the specimens tested at R = 0.1, very similar $\Delta K_{eff,th}$ values were obtained regardless of the grain size, suggesting that the effect of grain size on ΔK_{th} is minimized at low stress ratios as a result of crack closure. In contrast, the $\Delta K_{eff,th}$ values tended to decrease with decreasing grain size during the trials at R = 0.5 and 0.7. The slopes obtained from the data in Fig. 13 are

plotted in Fig. 14 to allow a better understanding of the grain size effect. These values exhibit an exponential increase as R is increased, demonstrating that the effect of grain size on $\Delta K_{eff,th}$ becomes more significant at higher stress ratios. It is therefore apparent that grain refinement significantly reduces $\Delta K_{eff,th}$ in CP titanium at relatively high stress ratios. The slopes obtained from the data of Ti-6Al-4V alloy were almost the same under various stress ratios [30]; therefore, the extent of grain size effect on $\Delta K_{eff,th}$ is dependent of materials.

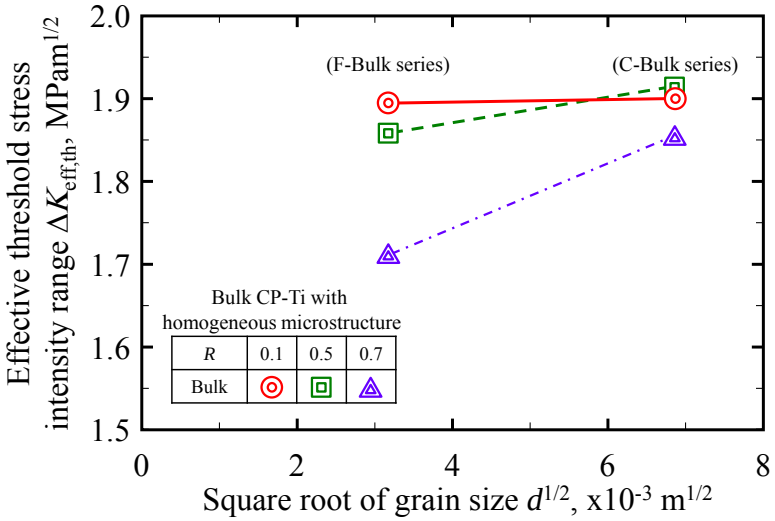

Fig.13 Relationship between effective threshold stress intensity range and square root of grain size.

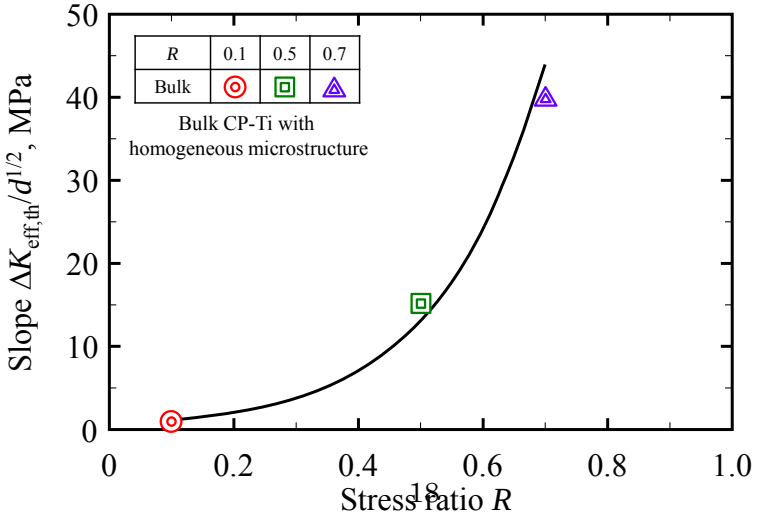

Fig.14 Relationship between slope and stress ratio.

Based on the above results and discussion, the effects of a bimodal harmonic structure on the fatigue threshold in CP titanium can be explained. Fig. 15 presents an illustration summarizing the mechanism by which the fatigue threshold in CP titanium is reduced as a consequence of the formation of a harmonic structure. In this figure, the fatigue threshold for the MM series is lower than that for the Untreated specimens because the harmonic structure has a fine grained microstructure, which exhibits low fatigue crack growth resistance. At low stress ratios, the fatigue threshold for the MM series is reduced due to a decrease in K_{cl} because of the presence of the fine grained structure. At high stress ratios, the effect of the grain size on ΔK_{th} becomes increasingly significant. Therefore, the fatigue threshold for the MM series is still reduced because of the decreased $\Delta K_{eff,th}$. Thus, the fatigue threshold for CP titanium is greatly reduced at high stress ratios due to the presence of the harmonic structure.

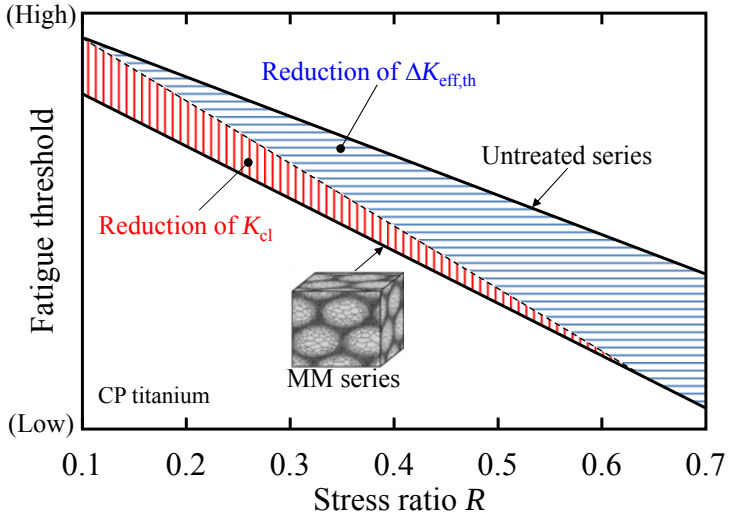

Fig.15 Schematic illustration of mechanism for reduction of fatigue threshold in CP titanium

following formation of harmonic structure.

5. Conclusions

The effect of a harmonic structure with a bimodal grain size distribution on near-threshold fatigue crack propagation in CP titanium was examined under various stress ratios. The effect of the grain size on near-threshold fatigue crack propagation was also investigated in order to determine the fatigue crack propagation mechanism in harmonic-structured CP titanium. The main conclusions obtained in this study can be summarized as follows:

1. The da/dN values in harmonic-structured CP titanium are higher than those in specimens fabricated from as-received powders with coarse grains for comparable values of ΔK.

2. The crack path in CP titanium is affected by the presence of a harmonic structure, thus decreasing the extent of roughness-induced crack closure.

3. The ΔK_{th} for harmonic-structured CP titanium is lower than that for material fabricated from as-received powders with coarse grains. This difference is attributed to a reduction in the extent of crack closure and $\Delta K_{eff,th}$ resulting from the presence of fine grains in the harmonic structure.

4. The fatigue crack growth resistance of CP titanium is significantly reduced for high stress ratios due to the presence of a harmonic structure. This phenomenon occurs because the effect of grain size on $\Delta K_{eff,th}$ becomes more significant with increasing stress ratio.

Acknowledgement

The authors would like to acknowledge financial support for this work by a JSPS KAKENHI Grant (Number 15K05677) and by The Light Metal Educational Foundation, Inc.

List of references

[1] Fleck C, Eifler D. Corrosion, fatigue and corrosion fatigue behaviour of metal implant materials, especially titanium alloys. Int. J. Fatigue 2010;32:929–935.

[2] Niinomi M. Mechanical properties of biomedical titanium alloys. Mater. Sci. Eng. A 1998;243:231-236.

[3] Niinomi M. Fatigue characteristics of metallic biomaterials. Int. J. Fatigue. 2007;29:992–1000.

[4] Rack HJ, Qazi JI. Titanium alloys for biomedical applications. Mater. Sci. Eng. C 2006;26:1269-1277.

[5] Teoh SH. Fatigue of biomaterials: a review. Int. J. Fatigue. 2000;22:825–837.

[6] Staiger MP, Pietak AM, Huadmai J, Dias G. Magnesium and its alloys as orthopedic biomaterials: A review. Biomater. 2006;27:1728-1734.

[7] Ikeo N, Nakamura R, Naka K, Hashimoto T, Yoshida T, Urade T, Fukushima K, Yabuuchi H, Fukumoto T, Ku Y, Mukai T. Fabrication of a magnesium alloy with excellent ductility for biodegradable clips. Acta Biomater. 2016;29:468-476.

[8] Sergueeva AV, Stolyarov VV, Valiev RZ, Mukherjee AK. Advanced mechanical properties of pure titanium with ultrafine grained structure. Scripta Mater. 2001;45:747-752.

[9] Ertorer O, Topping T, Li Y, Moss W, Lavernia EJ. Enhanced tensile strength and high ductility in cryomilled commercially pure titanium. Scripta Mater. 2009;60:586-589.

[10] Estrin Y, Vinogradov A. Fatigue behaviour of light alloys with ultrafine grain structure produced by severe plastic deformation: An overview. Int. J. Fatigue 2010;32:898-907.

[11] Kitahara H, Uchikado K, Makino J, Iida N, Tsushida M, Tsuji N, Ando S, Tonda H. Fatigue crack propagation behavior in commercial purity Ti severely deformed by accumulative roll bonding process. Mater. Trans. 2008;49:64–68.

[12] Kikuchi S, Yoshida S, Nakamura Y, Nambu K, Akahori T. Characterization of the hydroxyapatite layer formed by fine hydroxyapatite particle peening and its effect on the fatigue properties of commercially pure titanium under four-point bending. Surf. Coat. Technol. 2016;288:196-202.

[13] Morita T, Nakaguchi H, Noda S, Kagaya C. Effects of fine particle bombarding on surface characteristics and fatigue strength of commercial pure titanium. Mater. Trans. 2012;53:1938-1945.

[14] Terada D, Inoue S, Tsuji N. Microstructure and mechanical properties of commercial purity titanium severely deformed by ARB process. J. Mater. Sci. 2007;42:1673-1681.

[15] Terada D, Inoue M, Kitahara H, Tsuji N. Change in mechanical properties and microstructure of ARB processed Ti during annealing. Mater. Trans. 2008;49:41-46.

[16] Tsuji N, Kamikawa N, Ueji R, Takata N, Koyama H, Terada D. Managing both strength and ductility in ultrafine grained steels. ISIJ Int. 2008;48:1114-1121.

[17] Wang Y, Chen M, Zhou F, Ma E. High tensile ductility in a nanostructured metal. Nature 2002;419:912–915.

[18] Fang TH, Li WL, Tao NR, Lu K. Revealing extraordinary intrinsic tensile plasticity in gradient nano-grained copper. Science 2011;331:1587–1590.

[19] Peter JS, David PF, Bertalan J, Jelena H, Tamas U. Bimodal grain size distribution enhances strength and ductility simultaneously in a low-carbon low-alloy steel. Metallurgical Mater. Trans. A 2015;46A:1948-1957.

[20] Somekawa H, Singh A, Mukai T. High fracture toughness of extruded Mg–Zn–Y alloy by the synergistic effect of grain refinement and dispersion of quasicrystalline phase. Scripta Mater. 2007;56:1091-1094.

[21] Mimoto T, Umeda J, Kondoh K. Titanium powders via gas-solid direct reaction process and mechanical properties of their extruded materials. Mater. Trans. 2015;56:1153-1158.

[22] Mimoto T, Umeda J, Kondoh K. Strengthening behaviour and mechanisms of extruded powder metallurgy pure Ti materials reinforced with ubiquitous light elements. Powder Metall. 2016;59:223-228.

[23] Mimoto T, Kondoh K. Strengthening and toughening mechanisms of extruded pure titanium powder materials by adding ubiquitous light elements. Titanium Japan 2011;61:302-307.

[24] Sekiguchi T, Ono K, Fujiwara H, Ameyama K. New microstructure design for commercially pure titanium with outstanding mechanical properties by mechanical milling and hot roll sintering. Mater. Trans. 2010;51:39–45.

[25] Ota M, Vajpai SK, Imao R, Kurokawa K, Ameyama K. Application of high pressure gas jet mill process to fabricate high performance harmonic structure designed pure titanium. Mater. Trans. 2015;56:154-159.

[26] Fujiwara H, Sekiguchi T, Ameyama K. Mechanical properties of pure titanium and Ti-6Al-4V alloys with a new tailored nano/meso hybrid microstructure. Int. J. Mater. Res. 2009;100:796-799.

[27] Kikuchi S, Nakamura Y, Ueno A, Ameyama K. Low temperature nitriding of commercially pure titanium with harmonic structure. Mater. Trans. 2015;56:1807-1813.

[28] Kikuchi S, Hayami Y, Ishiguri T, Guennec B, Ota M, Ueno A, Ameyama K. Effect of bimodal grain size distribution on fatigue properties of Ti-6Al-4V alloy with harmonic structure under four-point bending. Mater. Sci. Eng. A 2017;687:269-275.

[29] Kikuchi S, Takemura K, Hayami Y, Ueno A, Ameyama K. Evaluation of the fatigue properties of Ti-6Al-4V alloy with harmonic structure in 4-points bending. J. Soc. Mater. Sci., Jpn. 2015;64:880-886.

[30] Kikuchi S, Imai T, Kubozono H, Nakai Y, Ota M, Ueno A, Ameyama K. Effect of harmonic structure design with bimodal grain size distribution on near-threshold fatigue crack propagation in Ti-6Al-4V Alloy. Int. J. Fatigue 2016;92:616-622.

[31] Kikuchi S, Imai T, Kubozono H, Nakai Y, Ueno A, Ameyama K. Evaluation of near-threshold fatigue crack propagation in Ti-6Al-4V alloy with harmonic structure created by mechanical milling and spark plasma sintering. Frattura ed Integrità Strutturale 2015;34:261-270.

[32] Nalla RK, Boyce BL, Campbell JP, Peters JO, Ritchie RO. Influence of microstructure on high-cycle fatigue of Ti-6Al-4V: bimodal vs. lamellar structures. Metall. Mater. Trans. A 2002;33:899–918.

[33] Boyce BL, Ritchie RO. Effect of load ratio and maximum stress intensity on the fatigue threshold in Ti-6Al-4V. Eng. Fract. Mech. 2001;68:129–147.

[34] Nakajima K, Terao K, Miyata T. The effect of microstructure on fatigue crack propagation of α+β titanium alloys in-situ observation of short fatigue crack growth. Mater. Sci. Eng. A 1998;243:176-181.

[35] Nakai Y, Tanaka K. The effects of stress ratio and grain size on near-threshold fatigue crack propagation in low-carbon steel. Eng. Fract. Mech. 1981;15:291–302.

[36] Sugeta A, Jono M, Uematsu Y, Yamamoto M, Ueda H. Effect of microstructure on fatigue crack growth behavior in Ti-6Al-4V alloy. J. Soc. Mater. Sci. Jpn. 1998;47:273–278.

[37] Oguma H, Nakamura T. The effect of stress ratios on very high cycle fatigue properties of Ti-6Al-4V,.Key Eng. Mater. 2004;261-263:1227-1232.

[38] Ogawa T, Tokaji K, Ohya K. The effect of microstructure and fracture surface roughness on fatigue crack propagation in a Ti-6Al-4V alloy. Fatigue Fract. Eng. Mater. Struct.,

1993;16:973–982.

[39] Sadananda K, Vasudevan AK. Fatigue crack growth behavior of titanium alloys. Int. J. Fatigue 2005;27:1255-1266.

[40] Tokizane M, Isonishi K. Production of uniformly-sized spherical powder by plasma rotating electrode process and its applications to some intermetallics powders. J. Jpn. Soc. Powder Metal. 1992;39:1137-1144.

[41] Ameyama K, Sekiguchi T. Creation of revolutionary new structure materials by harmonic structure design. J. Jpn. Soc. Heat Treat. 2013;53:1–2.

[42] Kikukawa M, Jono M, Tanaka K, Takatani M. Measurement of fatigue crack propagation and crack closure at low stress intensity level by unloading elastic compliance method. J. Soc. Mater. Sci., Jpn. 1976;25:899–903.

List of table and figure captions

Table 1 Average grain size and areal fraction of fine-grained structure in MM series.

Fig.1 Schematic illustration of process for formation of harmonic-structured material.

Fig.2 Flowchart of specimen preparation procedure.

Fig.3 Inverse pole figure maps obtained by EBSD analysis for (a) Untreated and (b) MM series.

Fig.4 Inverse pole figure maps obtained by EBSD analysis for (a) as-received material (C-Bulk series), (b) cold-rolled material, and (c) annealed material pre-treated with cold

rolling (F-Bulk series).

Fig.5 Relationship between crack growth rate and stress intensity range for various sintered compacts.

Fig.6 Relationship between threshold stress intensity range and stress ratio for various sintered compacts.

Fig.7 Relationship between crack growth rate and effective stress intensity range for various sintered compacts.

Fig.8 Relationship between K_{cl}/K_{max} and effective stress intensity range for various sintered compacts.

Fig.9 SEM micrographs of crack profiles for (a) Untreated and (b) MM series after testing at $R = 0.5$.

Fig.10 Axonometric drawings of fracture surfaces for (a) Untreated and (b) MM series after testing at $R = 0.1$.

Fig.11 Relationship between threshold stress intensity range and stress ratio for two types of bulk homogeneous materials.

Fig.12 Relationship between closure stress intensity factor and stress intensity range for two types of bulk homogeneous materials.

Fig.13 Relationship between effective threshold stress intensity range and square root of grain size.

Fig.14 Relationship between slope and stress ratio.

Fig.15 Schematic illustration of mechanism for reduction of fatigue threshold in CP titanium following formation of harmonic structure.